Available online at www.sciencedirect.com
SCIENCE DIRECT®
Journal of Photochemistry and Photobiology A: Chemistry 169 (2005) 47–55
Journal of Photochemistry and Photobiology A:Chemistry
www.elsevier.com/locate/jphotochem

Hydrogen-atom migration and Wolff rearrangement in photolysis of chlorohydroquinone to produce *p*-benzoquinone and 3-hydroxy-2,4-cyclopentadiene-1-ylidenemethanone

Nobuyuki Akai, Satoshi Kudoh, Munetaka Nakata*

Graduate School of BASE (Bio-Applications and Systems Engineering), Tokyo University of Agriculture and Technology, Naka-cho, Koganei, Tokyo 184-8588, Japan

Received 6 February 2004; received in revised form 22 April 2004; accepted 31 May 2004
Available online 29 July 2004

Abstract

Photolysis of chlorohydroquinone in a low-temperature argon matrix was investigated by Fourier transform infrared spectroscopy with an aid of hybrid density-functional-theory (DFT) calculation. The new photoreaction pathways via a ketocarbene intermediate produced by dissociation of hydrogen chloride upon UV irradiation were found, where a five-membered ring ketene and *p*-benzoquinone were produced from the ketocarbene by Wolff rearrangement and intramolecular hydrogen-atom migration, respectively. The large H/D isotope effect in the branching ratio for the final products, ketene and *p*-benzoquinone, was found in the analysis of the growth behavior of the infrared bands, implying that the hydrogen-atom migration occurs by tunneling effect.

Keywords: Matrix-isolation infrared spectroscopy; Chlorohydroquinone; Hydrogen-atom migration; Wolff rearrangement; Tunneling effect

1. Introduction

The photochemistry of halogen-atom substituted phenols is an important subject in environmental chemistry, because highly toxic compounds like dibenzo-*p*-dioxin and dibenzofuran are produced from the phenols [1–6]. Our recent study of the photolysis of 2-chlorophenol in low-temperature rare-gas matrices revealed that a five-membered ring ketene compound (2,4-cyclopentadiene-1-ylidenemethanone), here denoted as FK, was produced instead of dibenzo-*p*-dioxin by elimination of hydrogen chloride from 2-chlorophenol [7], as Scheme 1. This fact is ascribed to the lifetime of the ketocarbene intermediate and to its concentration in matrices. If this intermediate has a long enough lifetime, dibenzo-*p*-dioxin is produced by dimerization, while production of FK by the intramolecular electron rearrangement, i.e., Wolff rearrangement, overwhelms that of dibenzo-*p*-dioxin if the lifetime is much shorter. Our conclusion is that the lifetime of ketocarbene is too short to produce dibenzo-*p*-dioxin even in low-temperature rare-gas matrices with a relatively high concentration.

A similar experiment was performed for 2-bromphenol [8]. In this case, 4-bromo-2,5-cyclohexadienone is one of the final photoproducts besides FK (Scheme 2). The latter, a minor product, is produced from the same ketocarbene in the photolysis of 2-chlorophenol, while the pathway for production of the major product 4-bromo-2,5-cyclohexadienone is rather puzzling because intramolecular migrations of hydrogen and bromine atoms are required.

In the present study, we have investigated the photolysis of chlorohydroquinone, i.e., hydroxy-substituted 2-chlorophenol, to understand the reactivity of the ketocarbene produced by elimination of hydrogen chloride in comparison with the case in 2-chlorophenol. To identify the final products, the measured infrared spectra are analyzed with reference to the calculated spectral patterns of possible species by the density-functional-theory (DFT) method. Our main purpose is to elucidate the competitive reaction pathways for intramolecular hydrogen-atom migration and Wolff rearrangement of the intermediate in the photolysis of chlorohydroquinone.

2. Experimental and calculation methods

Chlorohydroquinone was purchased from Tokyo Chemical Industry Co. Ltd., and chlorohydroquinone-d_2 (-OD) was

* Corresponding author. Tel./fax: +81-42-388-7349.
E-mail address: necom@cc.tuat.ac.jp (M. Nakata).

1010-6030/$ – see front matter © 2004 Elsevier B.V. All rights reserved.
doi:10.1016/j.jphotochem.2004.05.033

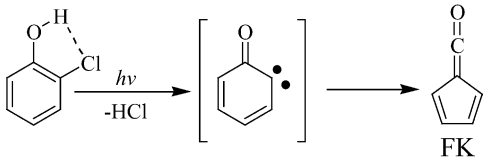

Scheme 1.

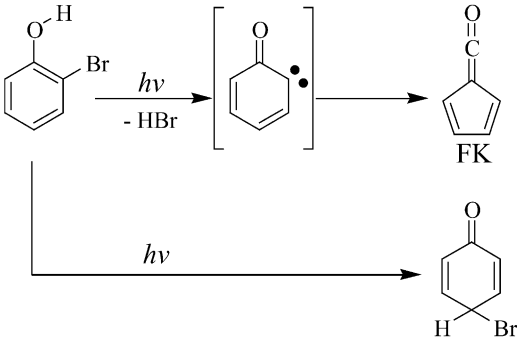

Scheme 2.

synthesized by mixing chlorohydroquinone with an excess amount of D_2O. Each sample placed in a deposition nozzle with a heating system was vaporized at 310 K. Pure argon (Nippon Sanso, 99.9999% purity) was flowed over the sample, and the flow rate of argon gas was adjusted to obtain sufficient isolation. The mixed gas was expanded through a stainless steel pipe of 1/16 in. in diameter and deposited in a vacuum chamber on a CsI plate, cooled at about 16 K by a closed cycle helium refrigeration unit (CTI Cryogenics, Model M-22). UV radiation from a superhigh-pressure mercury lamp was used to induce photoreaction, where a water filter to remove thermal reactions and UV-28, UV-30 and UV-32 short-wavelength cutoff filters (HOYA) to choose irradiation wavelengths were used. Infrared spectra of the matrix samples were measured with an FTIR spectrophotometer (JEOL, Model JIR-7000). The band resolution was 0.5 cm^{-1}, and the number of accumulation was 64. Other experimental details were reported elsewhere [9,10].

Density-functional-theory calculations with the 6–31++G** basis set were carried out using the GAUSSIAN 98 program [11]. The hybrid density functional [12], in combination with the Lee–Yang–Parr correlation functional (B3LYP) [13], was used to optimize geometrical structures.

3. Results and discussion

3.1. Infrared spectrum of chlorohydroquinone

Fig. 1(a) shows the infrared spectrum of chlorohydroquinone isolated in an argon matrix at 16 K measured after deposition and before UV irradiation. The bands appearing at around 1500 and 1150 cm^{-1} are due to the benzene-ring stretching and in-plane hydrogen bending modes, respectively. These bands exhibit multiple peaks, implying that more than one conformer exists in the matrix.

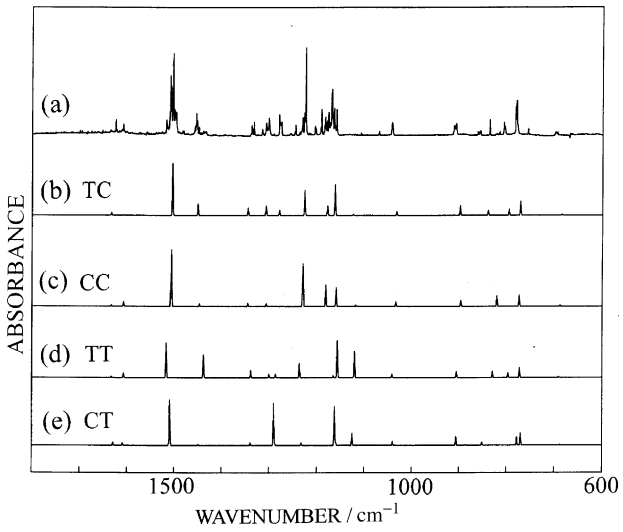

Fig. 1. Infrared spectrum of chlorohydroquinone. (a) Observed spectrum in an argon matrix and calculated spectral patterns for four possible conformers; (b) TC, (c) CC, (d) TT and (e) CT.

Chlorohydroquinone has *cis* and *trans* conformations around the two C–OH bonds, resulting in four possible conformers: TC, CC, TT and CT, shown in Fig. 2; the first letter denotes *trans* (T) or *cis* (C) hydroquinone, while the second letter denotes *trans* (T) or *cis* (C) conformation around the H–O–C=C–Cl part. A DFT calculation at the DFT/B3LYP/6–31++G** level results in that the optimized geometry for TC and CC is more stable than that for TT and CT because of the intramolecular hydrogen bond between the O–H and C–Cl groups, the relative energies being calculated to be 0 (TC), 0.47 (CC), 12.6 (TT) and 13.5 kJ mol^{-1} (CT). The stabilization energy due to the hydrogen bond is almost consistent with that for 2-chlorophenol (13.1 kJ mol^{-1}) [7]. On the other hand, the energy difference between TC and CC (0.47 kJ mol^{-1}) is nearly equal to that for its parent molecule, hydroquinone, where the *trans* conformation is more stable than the *cis* by 0.56 kJ mol^{-1} [14]. According to the Boltzmann distribution law at the deposition temperature of 310 K, the population ratio of TC/CC/TT/CT is calculated to be 100/83.2/0.7/0.5. It is then reasonable to assume that the observed spectrum is mainly composed of the bands of the TC and CC

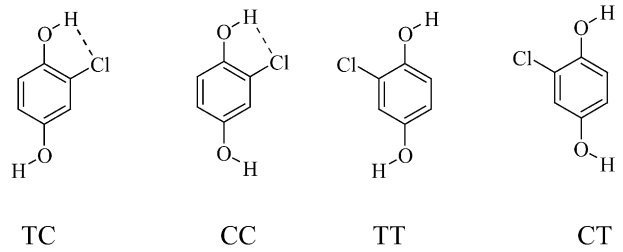

Fig. 2. Four possible conformations of chlorohydroquinone.

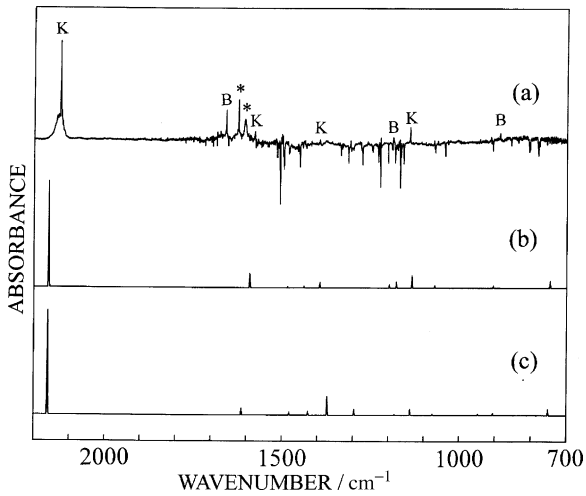

Fig. 3. (a) A difference spectrum, after minus before UV irradiation, through a UV-28 short-wavelength cutoff filter for 1 min. A band marked with * is due to H_2O in the matrix. Bands marked with B are assigned to *p*-benzoquinone and K to HO-FK. (b) and (c) Calculated spectral patterns for *cis* and *trans* HO-FK, respectively.

conformers. The spectral patterns of the four conformers obtained by the DFT/B3LYP/6–31++G** method are compared with the observed spectrum in Fig. 1, where a scaling factor of 0.98 is used. The calculated patterns of TC and CC seem to be consistent with the observed spectrum. We tried to distinguish the TC and CC bands in the observed spectrum by raising the matrix temperature from 16 to 28 K to induce the thermodynamical isomerization between TC and CC, but no spectral change was observed in contrast to the case of hydroquinone [14]. Thus, we assumed in the subsequent kinetic analysis that nearly equal amounts of the TC and CC bands are overlapped with each other.

3.2. Identification of photoproducts

3.2.1. (a) 3-Hydroxy-2,4-cyclopentadiene-1-ylidenemethanone

When the matrix sample was exposed to UV light from the mercury lamp, the photolysis of chlorohydroquinone occurred immediately. Fig. 3(a) shows a difference spectrum between spectra measured after and before 1-min UV irradiation through the UV-28 filter ($\lambda > 270$ nm), where the increasing and decreasing bands are assignable to products and the reactant, respectively. The sharp and intense band appearing at 2126 cm^{-1}, marked with K, is assigned to the C=C=O stretching vibrational mode of a ketene compound. The 1579, 1396 and 1140 cm^{-1} bands marked with K are also assignable to the ketene, since they show the same growth behavior as the 2126 cm^{-1} band. The bands marked with B are assigned to *p*-benzoquinone, as described later.

In our previous study of 2-chlorophenol in a low-temperature matrix [7], FK was produced by photodissociation of hydrogen chloride, as shown in Scheme 1. If a similar reaction occurs in the photolysis of chlorohydroquinone,

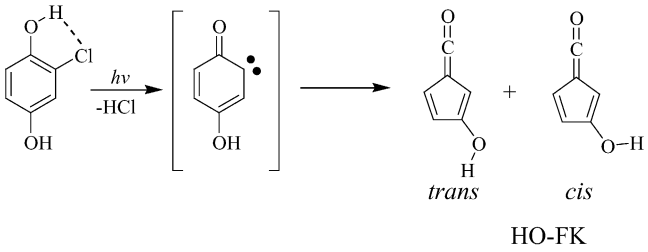

Scheme 3.

formation of 3-hydroxy-2,4-cyclopentadiene-1-ylidenemethanone, here denoted as HO-FK, is expected as shown in Scheme 3.

HO-FK has two conformations around the C–OH bond, *trans* and *cis*, where *cis* is more stable by 3.4 kJ mol^{-1}. The calculated spectral patterns of *trans* and *cis* HO-FK are compared with the observed spectrum in Fig. 3. The K bands can be assigned to *cis* but not *trans* HO-FK. For example, the wavenumbers and the relative intensity of the bands appearing at 1579, 1396 and 1140 cm^{-1} correspond to that of the 1591, 1394 and 1134 cm^{-1} bands of *cis*, respectively. No *trans* bands are observed despite a small energy difference of 3.4 kJ mol^{-1}; for example, the second intense band of *trans* expected to appear at 1372 cm^{-1} is missing in the observed spectrum. This finding raises the question on whether or not the conformational isomerization around the C–OH bond occurs in a low-temperature rare-gas matrix. Since the isomerization barrier scaled from the potential minimum of *trans* is estimated to be ca. 9.8 kJ mol^{-1} by the DFT calculation, the thermodynamical isomerization from *trans* to *cis* in a low-temperature matrix seems to be difficult [15]. Another possibility is that *trans* is converted to *cis* by hydrogen-atom tunneling, as discussed later in Section 3.4.

The observed and calculated wavenumbers of HO-FK, which is a hitherto unknown molecule, are summarized in Table 1. The 1062 and 913 cm^{-1} bands are also assigned to HO-FK, although their intensities are much weaker than the rest. The band observed at 2857 cm^{-1} is assigned to the co-product HCl, which interacts with FK as reported elsewhere [7].

3.2.2. (b) p-Benzoquinone–HCl complex

When a matrix sample was exposed to UV light for a prolonged time, the intensity of the B bands increased, while that of the K bands, assigned to the HO-FK bands, decreased. Fig. 4 shows spectral changes ranging between 1600 and 2200 cm^{-1}. The growth behavior of the 1659 cm^{-1} C=O stretching band is totally different from that of the HO-FK C=C=O stretching band, 2126 cm^{-1}. The difference between the spectrum measured after UV irradiation for 180 min and that after 60 min is shown in Fig. 5(a). The HO-FK bands marked with K decreased in this period, while those marked with B increased. The pattern of the B bands is similar, though not identical, to that of *p*-benzoquinone reported in [16–18]. This finding suggests that the B bands

Table 1
Observed and calculated wavenumbers (in cm^{-1}) of HO-FK, 3-hydroxy-2,4-cyclopentadiene-1-ylidenemethanone, with their relative intensities

Observed		Calculated			
		Cis		*Trans*	
v	Int.	*v*[a]	Int.	*v*[a]	Int.
		3754	4.5	3768	6.2
		3201	0.1	3211	0.2
		3190	0.3	3198	0.1
		3181	0.0	3156	0.4
2126	100	2158	100	2160	100
1579	11.3	1591	13.4	1613	6.6
		1485	1.3	1479	3.0
		1439	1.6	1426	4.0
1396	5.7	1394	5.2	1372	18.1
		1293	0.1	1296	5.9
		1198	3.4	1200	0.3
		1178	5.9	1182	1.3
1140	15.9	1134	11.8	1138	5.9
1062	2.9	1070	2.4	1075	1.6
		952	0.3	947	1.7
913	2.7	905	2.2	905	2.2
		873	0.0	851	0.0
		746	6.6	751	6.0
		671	1.1	669	1.4
		649	0.0	653	0.8
		637	0.9	637	0.5
		613	1.3	607	1.2
		551	0.8	556	0.5
		505	0.2	506	0.0
		460	0.3	465	0.5
		396	0.9	395	0.7
		334	6.5	293	0.3
		287	2.1	204	8.3
		135	0.2	135	0.1
		102	0.0	99	0.0

[a] DFT/B3LYP/6–31++G** level calculation. A scaling factor of 0.98 is used.

are assignable to *p*-benzoquinone–HCl complex instead of *p*-benzoquinone monomer.

Fig. 5(b) and (c) shows the calculated spectral patterns of *p*-benzoquinone monomer and its complex with HCl, respectively. The hydrogen bond length (>C=O–H–Cl) of the optimized geometrical structure for this complex is calculated to be 1.85 Å, which is shorter than that for HO-FK–HCl complex (>C=C=O–H–Cl, ca. 2.2 Å), implying that the hydrogen bond in the former is stronger than that in the latter. By a comparison of the observed spectrum with the two calculated patterns, we conclude that the B bands are due to *p*-benzoquinone–HCl complex. Especially, the calculated pattern for the complex satisfactorily reproduces the C=O stretching region around 1700 cm^{-1}, where the two C=O stretching bands for *p*-benzoquinone appearing at 1671 and 1659 cm^{-1} are assignable to the symmetric (1705 cm^{-1}) and the asymmetric (1684 cm^{-1}) stretching modes; the former becomes infrared-active by perturbation of the hydrogen bond with HCl. The infrared band for HCl in the complex appearing at 2540 cm^{-1} shows a band as broad as ca. 40 cm^{-1} and has a shift as large as ca. 350 cm^{-1} from that of HCl monomer [7]. These findings support a strong intermolecular hydrogen bond in the *p*-benzoquinone–HCl complex. The observed and calculated wavenumbers for the monomer and the complex are summarized in Table 2 with their relative intensities.

3.3. Mechanism of photoreaction

The DFT calculation shows that *p*-benzoquinone is more stable than *cis* HO-FK by 67.3 kJ mol^{-1}. The photoreaction pathway to produce *p*-benzoquinone and HO-FK from chlorohydroquinone is summarized in Scheme 4.

The reaction intermediate, ketocarbene, is produced from chlorohydroquinone by elimination of HCl upon UV irradiation. This ketocarbene is a common precursor for HO-FK and *p*-benzoquinone; the former is produced by Wolff rearrangement, as in the photolysis of 2-chlorophenol, while the latter by intramolecular hydrogen-atom migration from the hydroxyl group. We assume that CO dissociates from HO-FK, because the 2126 cm^{-1} band decreases while the CO band at 2134 cm^{-1} increases after prolonged UV irradiation, as shown in Fig. 4.

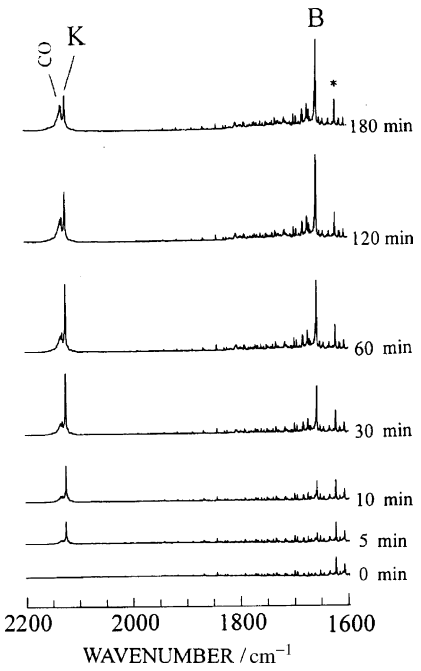

Fig. 4. Spectral changes for *p*-benzoquinone (B), HO-FK (K) and carbon monoxide (CO) upon UV irradiation time. A band marked with * represents a small amount of H_2O in the matrix.

The rate constants defined in Scheme 4 correspond to $\epsilon_{UV} \times \phi \times I$, where ϵ_{UV}, ϕ and I represent the decadic extinction coefficient, the reaction quantum efficiency and the UV photon intensity, respectively [19]. This expression for the rate constants holds in the weak absorption limit, which in our analysis is applicable to chlorohydroquinone and HO-FK. To determine the rate constants k_1, k_2 and k_3, the dependence of the absorbance of the 1224, 2126 and 1659 cm^{-1} bands assigned to chlorohydroquinone, HO-FK and *p*-benzoquinone

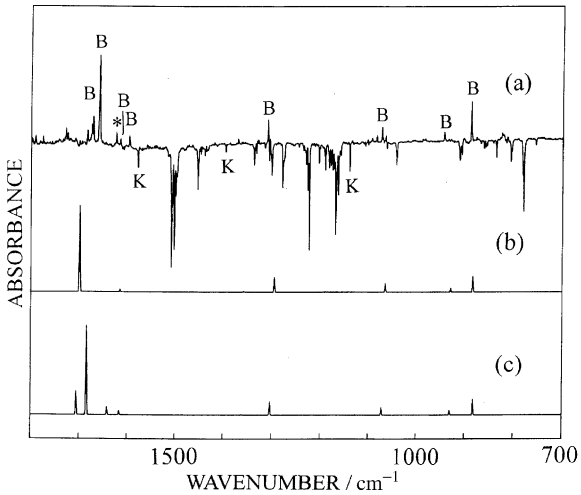

Fig. 5. (a) A difference spectrum after 180-min minus 60-min UV irradiation through a UV-28 short-wavelength cutoff filter. See the caption of Fig. 3 for symbols *, B and K. (b) and (c) Calculated spectral patterns for *p*-benzoquinone monomer and its complex with hydrogen chloride, respectively.

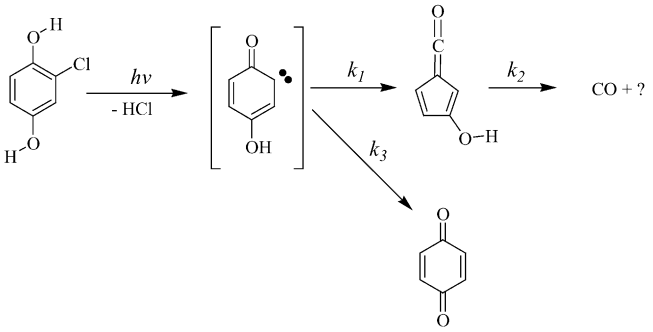

Scheme 4.

on the irradiation time was examined. By solving the rate equations, we obtain the following equations involving the irradiation time t

$$\frac{A_R}{\varepsilon_R} = [R] = (a_0 - a_\infty) \times \exp\{-(k_1 + k_3) \times t\} + a_\infty, \quad (1)$$

$$\frac{A_K}{\varepsilon_K} = [K] = (a_0 - a_\infty) \times \frac{k_1}{k_1 + k_3 - k_2} \times [\exp(-k_2 \times t) - \exp\{-(k_1 + k_3) \times t\}], \quad (2)$$

$$\frac{A_B}{\varepsilon_B} = [B] = (a_0 - a_\infty) \times \frac{k_3}{k_1 + k_3} \times [1 - \exp\{-(k_1 + k_3) \times t\}], \quad (3)$$

where $[R]$, $[K]$ and $[B]$ represent the numbers of molecules for chlorohydroquinone, HO-FK and *p*-benzoquinone, respectively, obtained from the integrated absorbance A_x divided by the corresponding infrared absorption coefficient ε_x. Since no experimental information on ε_x is available, the calculated intensities obtained by the DFT method, 187, 1359 and 447 km mol^{-1} for the 1224, 2126 and 1659 cm^{-1} bands respectively, are assumed, where the averaged value of the TC (137 km mol^{-1}) and CC (236 km mol^{-1}) conformers is used for chlorohydroquinone. The constant a_0, representing the initial number of reactant molecules, chlorohydroquinone, can be estimated from the A_x value measured before UV irradiation. The constant a_∞ represents the number of reactant molecules remaining after UV irradiation by the distortion of the matrix cage. This constant is treated as a variable parameter in the least-squares fitting.

The calculated dependence of the relative number of molecules on the irradiation time, shown in Fig. 6 by solid lines, are consistent with the corresponding observed values within experimental error. The intensity of the reactant decreases exponentially, and *p*-benzoquinone is produced more rapidly than HO-FK. The observed value of k_3 is roughly twice as large as that of k_1, as listed in Table 3.

3.4. Intramolecular hydrogen-atom migration

The photoinduced hydrogen-atom migration in carbenes has been investigated by low-temperature matrix-isolation

Table 2
Observed and calculated wavenumbers (in cm^{-1}) of *p*-benzoquinone (*p*-BQ), monomer and complex with hydrogen chloride

Observed				Calculated				
p-BQ monomer[a]		This work		Monomer			Complex	
v	Int.	*v*	Int.	*v*[b]	Int.	Sym.	*V*[b]	Int.
				3151	0	a_g	3155	0.1
				3149	1.0	b_{2u}	3153	0.2
				3133	0	b_{3g}	3139	0.1
				3133	0.4	b_{1u}	3138	0.1
		2540[c]	23.2				2573	265
1672[d]	70	1671	34.5	1701	0	a_g	1705	26.1
1659[d]	52	1659	100	1699	100	b_{1u}	1684	100
		1624	15.5	1645	0	a_g	1641	8.8
1596	9	1597	11.5	1615	3.8	b_{2u}	1616	4.5
				1371	0	b_{3g}	1374	0.2
1357[e]	4.7	1371	4	1358	1.1	b_{1u}	1361	0.7
1301	3	1309	22.6	1295	17.6	b_{2u}	1303	15.0
				1213	0	b_{3g}	1218	0.1
				1145	0	a_g	1151	0.1
1066	17	1073	16.9	1065	10.0	b_{2u}	1072	8.4
				990	0	b_{2g}	991	0.0
				989	0	a_u	990	0.0
942	9	943	11.6	929	4.3	b_{1u}	930	5.2
886	50	888	49.9	883	18.6	b_{3u}	882	17.4
				766	0	b_{2g}	764	0.1
				759	0	a_g	759	0.1
				740	0.1	b_{1u}	744	0.4
				740	0	b_{1g}	743	0.0
				589	0	b_{3g}	594	0.2
							548	18.3
503	2.9			504	1.0	b_{3u}	508	0.0
							496	7.7
				447	0	b_{3g}	452	2.2
				445	0	a_g	447	0.5
407	18			404	5.6	b_{2u}	408	9.1
				330	0	a_u	331	0.0
				219	0	b_{2g}	217	0.1
				117	2.8			
				93	3.4	b_{3u}	93	2.1
				37	0.2			

[a] Ref. [17].
[b] DFT/B3LYP/6–31++G** level calculation. A scaling factor of 0.98 is used.
[c] Broad band assigned to H–Cl stretching mode.
[d] Multiple band splittings – 1755, 1707, 1682, 1672, 1670, 1659 and 1640 cm^{-1} – due to Fermi resonance.
[e] A shoulder band appears at 1353 cm^{-1}.

spectroscopy [20–25]. For example, *o*-tolyldiazomethane is converted to *o*-xylylene via *o*-tolylcarbene by UV photolysis, as shown in Scheme 5 [20]. McMahon and Chapman examined the H/D isotope effect for the hydrogen migration and claimed the possibility of hydrogen tunneling.

Table 3
Rate constants (in min^{-1}) for chlorohydroquinone

	Normal species	Deuterated species
k_1	0.007 ± 0.001[a]	[b]
k_2	0.013 ± 0.003	[b]
k_3	0.013 ± 0.001	[b]
$k_1 + k_3$	0.020 ± 0.002	0.022 ± 0.003

[a] Uncertainty represents three times standard derivations in least-squares fitting.
[b] Not determined independently.

On the other hand, Tomioka et al. reported *o*-quinone-type molecules produced by hydrogen-atom migration. For example, 2-hydroxyphenylazide and 2-aminophenylazide are converted to *o*-benzoquinonemonoimine (6-imino-2,4-cyclohexadiene-1-one) and *o*-benzoquinonediimine (1,2-diimino-3,5-cyclohexadine), respectively [22–24] (Scheme 6).

To solve the question on whether hydrogen-atom migration in the photolysis of chlorohydroquinone originates from tunneling, we performed a similar experiment for deuterated chlorohydroquinone. The observed infrared spectrum of deuterated chlorohydroquinone is very complicated, because the partially deuterated sample used contained four isotopic species in the matrix: normal, two kinds of one-OD (Isotopes I and II) and two-OD (Isotope III) species (see Scheme 7).

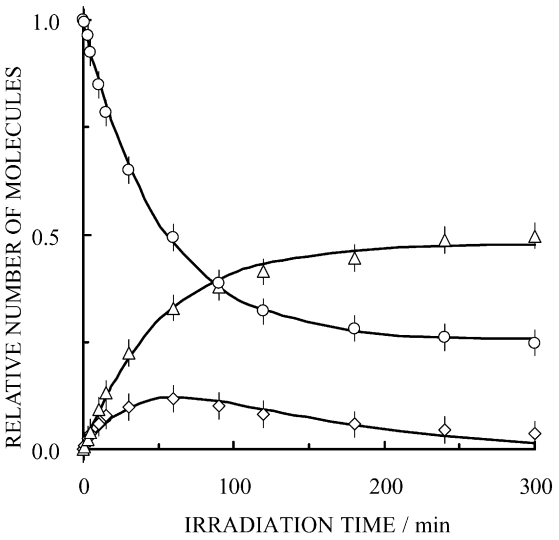

Fig. 6. Dependence of relative number of molecules on irradiation time, derived from the integrated infrared absorbance normalized by the calculated intensities and the initial observed value of the reactant, a_0. Symbols (○) represent chlorohydroquinone, (◇) HO-FK and (△) *p*-benzoquinone.

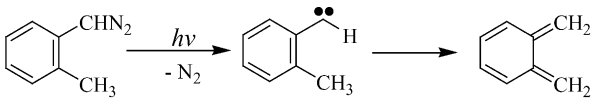

Scheme 5.

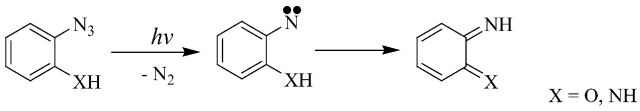

Scheme 6.

The infrared spectrum of the O–H and O–D stretching regions, shown in Fig. 7, is compared with that of the normal species. Two bands appear in each region, where the low- and high-wavenumber bands are assigned to the stretching modes with and without perturbation of the hydrogen bond between the O–H (or O–D) and C–Cl groups, respectively.

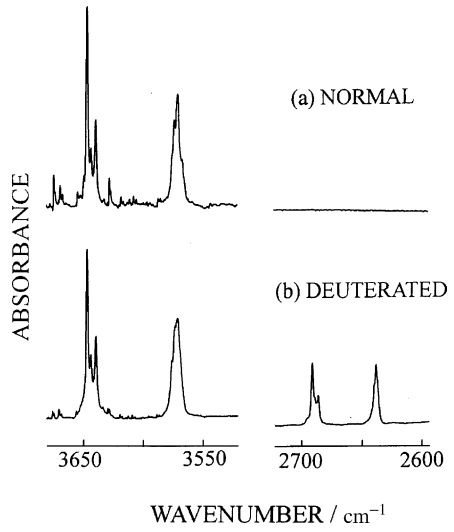

Fig. 7. Infrared spectra of O–H and O–D stretching regions: (a) normal and (b) deuterated chlorohydroquinones.

The two bands exhibit splittings due to either the matrix-site effect or Fermi resonance. One may expect that each of these peaks can be assigned to the bands of the TC and CC conformers. This is not the case, however, because the DFT calculation shows that the wavenumber difference between TC (3834 cm^{-1}) and CC (3833 cm^{-1}) is only 1 cm^{-1}. The band shapes of the O–H stretching region for the deuterated species are also very similar. Hence, we assume that the free O–H stretching band, ca. 3650 cm^{-1}, is composed of both Normal and Isotope I, while the hydrogen-bonding O–H stretching band, ca. 3570 cm^{-1}, is composed of both Normal and Isotope II. Similarly, we assume that the free O–D stretching, ca. 2690 cm^{-1}, is composed of Isotopes II + III, while the hydrogen-bonding bands, ca. 2630 cm^{-1}, is composed of Isotopes I + III.

The population ratio of (Normal + Isotope I)/(Isotopes II + III) in the sample can be estimated from the observed absorbance ratio of the free O–H and O–D stretching modes, if the corresponding absorption coefficients are known. Using

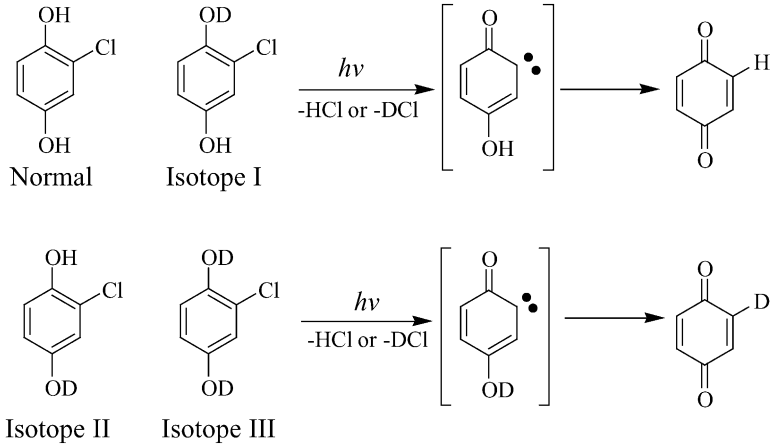

Scheme 7.

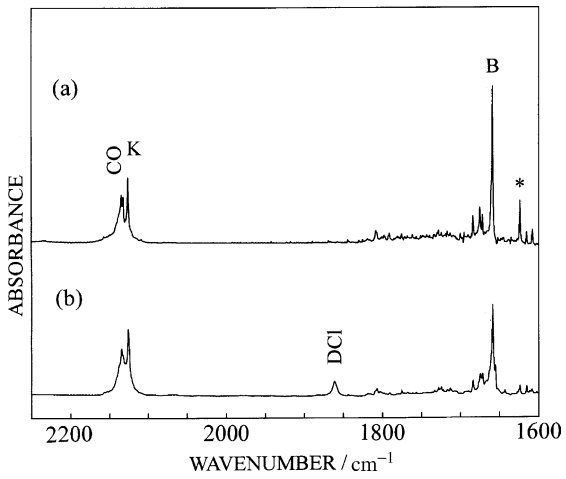

Fig. 8. Infrared spectra after 180-min UV irradiation through a UV-28 short-wavelength cutoff filter: (a) normal and (b) deuterated chlorohydroquinones. A band marked with * represents a small amount of H_2O in the matrix.

the calculated intensities obtained by the DFT calculation, about 65 km mol^{-1} for Normal and Isotope I, and about 42 km mol^{-1} for Isotopes II and III, the population ratio is estimated to be 2.1 from the observed integrated absorbance ratio of 3.2 by division of the calculated intensity ratio of 65/42.

When the deuterated matrix sample was exposed to UV light through the UV-28 cutoff filter, a similar photoreaction was observed. The D–Cl produced by photodissociation appeared at 1861 cm^{-1}. The decreasing rate constant of the deuterated reactant, $k_1 + k_3$, is thus determined to be 0.022 ± 0.003 from the absorbance change of the 2690 cm^{-1} band by a least-square fitting. This value is consistent with that of the O–H stretching band for the normal sample 0.020 ± 0.002. This means that the production rate for the ketocarbene intermediate is independent of deuteration. On the other hand, the production rate for the final products, i.e., the branching ratio between HO-FK and *p*-benzoquinone, depends on deuteration as shown in Fig. 8, where the relative intensity of *p*-benzoquinone (1659 cm^{-1}) against HO-FK bands (2126 cm^{-1}) in the deuterated sample is smaller than that of the normal sample. The DFT calculation shows that the C=O stretching band intensities are 476 and 571 km mol^{-1} for normal *p*-benzoquinone interacted with HCl and DCl, respectively, while 454 and 557 km mol^{-1} for *p*-benzoquinone-d_1 with HCl and DCl, respectively. This suggests that the C=O band for the deuterated species (Fig. 8(b)) is stronger than that for the normal species (Fig. 8(a)), if the amounts of the deuterated and normal species are equal. However, the result is opposite, which means that the migration of deuterium atom producing *p*-benzoquinone-d_1 is more difficult than the hydrogen-atom migration. This phenomenon may in principle be ascribed to hydrogen-atom tunneling, and our proposition may be verified by determination of k_1, k_2 and k_3 from the growth behavior of the normal and deuterated species for *p*-benzoquinone and HO-FK. In reality, however, it is impossible because the bands of the deuterated species are overlapped with those of the normal species, as shown in Fig. 8.

As for the possibility of the tunneling isomerization around the C–OH bond for HO-FK suggested in Section 3.2, the tunneling effect has been investigated by low-temperature matrix isolation for the OH torsional modes of several molecules such as formic acid [26–28], 3-hydroxypropadienylidene [29] and hydroquinones [14,30,31]. If the *cis–trans* isomerization of HO-FK occurs by tunneling, the *trans* bands may be observed in the spectrum of the deuterated matrix sample, because the deuterium-atom migration from *trans* to *cis* is slow. However, our infrared spectrum of a mixture of the normal and three isotope species is too complicated to detect the *trans* bands. Complete deuteration is essential to confirm the tunneling effect in HO-FK.

Acknowledgements

The authors thank Professor Kozo Kuchitsu (Tokyo University of Agriculture & Technology) for his helpful discussion.

References

[1] D.G. Crosby, A.S. Wong, Chemosphere 5 (1976) 327.
[2] P. Boule, C. Guyon, J. Lemaire, Chemosphere 11 (1982) 1179.
[3] P. Boule, C. Guyon, J. Lemaire, Chemosphere 13 (1984) 603.
[4] Y.I. Skurlatov, L.S. Ernestova, E.V. Vichutinskaya, D.P. Samsonov, I.V. Semenova, I.Y. Rod'ko, V.O. Shvidky, R.I. Pervunina, T.J. Kenp, J. Photochem. Photobiol. A 107 (1997) 207.
[5] Y. Okamoto, M. Tomonari, J. Phys. Chem. A 103 (1999) 7686.
[6] K. Ballschmiter, R. Bacher, Dioxine Chemie, Analytik, Vorkommen, Umweltverhalten und Toxkologie der halogenierten Dibenzo-*p*-dioxine und Dibenzofurane, Weinheim New York Basel Cambridge Tokyo, VCH, 1996.
[7] N. Akai, S. Kudoh, M. Takayanagi, M. Nakata, J. Photochem. Photobiol. A 146 (2001) 49.
[8] N. Akai, S. Kudoh, M. Nakata, Chem. Phys. Lett. 363 (2002) 591.
[9] M. Nakata, S. Kudoh, M. Takayanagi, T. Ishibashi, C. Kato, J. Phys. Chem. 104 (2000) 11304.
[10] N. Akai, S. Kudoh, M. Nakata, J. Phys. Chem. A 107 (2003) 2635.
[11] M.J. Frisch, G.W. Trucks, H.B. Schlegel, G.E. Scuseria, M.A. Robb, J.R. Cheeseman, V.G. Zakrzewski, J.A. Montgomery, R.E. Stratmann, J.C. Burant, S. Dapprich, J.M. Millam, A.D. Daniels, K.N. Kudin, M.C. Strain, O. Farkas, J. Tomasi, V. Barone, M. Cossi, R. Cammi, B. Mennucci, C. Pomelli, C. Adamo, S. Clifford, J. Ochterski, G.A. Peterson, P.Y. Ayala, Q. Cui, K. Morokuma, D.K. Malick, A.D. Rabuck, K. Raghavachari, J.B. Foresman, J. Cioslowski, J.V. Ortiz, B.B. Stefanov, G. Liu, A. Liashenko, P. Piskorz, I. Komaromi, R. Gomperts, R.L. Martin, D.J. Fox, T. Keith, M.A. Al-Laham, C.Y. Peng, A. Nanayakkara, C. Gonzalez, M. Challacombe, P.M.W. Gill, B.G. Johnson, W. Chen, M.W. Wang, J.L. Andres, M. Head-Gordon, E.S. Replogle, J.A. Pople, Gaussian98 (Revision A.6), Gaussian, Inc., Pittsburgh, PA, 1998.
[12] A.D. Becke, J. Chem. Phys. 98 (1993) 5648.
[13] C. Lee, W. Yang, R.G. Parr, Phys. Rev. B 37 (1988) 785.
[14] N. Akai, S. Kudoh, M. Takayanagi, M. Nakata, Chem. Phys. Lett. 356 (2002) 133.

[15] A.J. Barnes, J. Mol. Struct. 113 (1984) 161.
[16] W. McCarthy, A.M. Plokhotnichenko, E.D. Radchenko, J. Smets, D.M.A. Smith, S.G. Stepanian, L. Adamowicz, J. Phys. Chem. A 101 (1997) 7208.
[17] A.M. Plokhotnichenko, E.D. Radchenko, S.G. Stepanian, L. Adamowicz, J. Phys. Chem. A 103 (1999) 11052.
[18] C.-G. Zhan, S. Iwata, Chem. Phys. 230 (1998) 45.
[19] M. Nakata, H. Frei, J. Am. Chem. Soc. 111 (1989) 5240.
[20] R.J. McMahon, O.L. Chapman, J. Am. Chem. Soc. 109 (1987) 683.
[21] J. Morawietz, W. Sander, M. Traeubel, J. Org. Chem. 60 (1995) 6368.
[22] H. Tomioka, T. Matsushita, S. Murata, S. Koseki, Liebigs Ann. (1996) 1971.
[23] H. Tomioka, Pure Appl. Chem. 69 (1997) 837.
[24] H. Tomioka, Bull. Chem. Soc. Jpn. 71 (1998) 1501.
[25] H. Wandel, W. Sander, Eur. J. Org. Chem. (1999) 1005.
[26] M. Pettersson, E.M.S. Maçôas, L. Khriachtchev, J. Lundell, R. Fausto, M. Räsänen, J. Chem. Phys. 117 (2002) 9095.
[27] M. Pettersson, E.M.S. Maçôas, L. Khriachtchev, R. Fausto, M. Räsänen, J. Am. Chem. Soc. 125 (2003) 4058.
[28] E.M.S. Maçôas, L. Khriachtchev, M. Pettersson, J. Juselius, R. Fausto, M. Räsänen, J. Chem. Phys. 119 (2003) 11765.
[29] J. Szczepanski, S. Ekern, M. Vala, J. Phys. Chem. 99 (1995) 8002.
[30] N. Akai, S. Kudoh, M. Takayanagi, M. Nakata, J. Phys. Chem. A 106 (2002) 11029.
[31] N. Akai, S. Kudoh, M. Nakata, J. Phys. Chem. A 107 (2003) 3655.